PHARMACIA

Pharmacia 71: 1–12
DOI 10.3897/pharmacia.71.e124099

Research Article

In silico investigation of potential interleukin-8 (IL-8) and Cathelicidin (LL-37) inhibitors for rosacea treatment

Taufik Muhammad Fakih[1,2], Deis Hikmawati[3], Endang Sutedja[4], Reiva Farah Dwiyana[4], Nur Atik[5], Muchtaridi Muchtaridi[1,6]

1 *Department of Pharmaceutical Analysis and Medicinal Chemistry, Faculty of Pharmacy, Universitas Padjadjaran, Jalan Raya Bandung-Sumedang KM 21, Sumedang 45363, Indonesia*
2 *Department of Pharmacy, Faculty of Mathematics and Natural Sciences, Universitas Islam Bandung, Jl. Ranggagading No.8, Bandung 40116, Indonesia*
3 *Department of Dermatology, Faculty of Medicine, Universitas Islam Bandung, Jl. Tamansari No.20, Bandung 40116, Indonesia*
4 *Department of Dermatology and Venereology, Faculty of Medicine, Universitas Padjadjaran-Dr. Hasan Sadikin Hospital, Jl. Pasteur 38, Bandung 40161, Indonesia*
5 *Department of Biomedical Sciences, Faculty of Medicine, Universitas Padjadjaran, Jalan Raya Bandung-Sumedang KM 21, Sumedang 45363, Indonesia*
6 *Research Collaboration Centre for Theranostic Radio Pharmaceuticals, National Research and Innovation Agency (BRIN), Jl. Raya Bandung-Sumedang KM 21, Sumedang 45363, Indonesia*

Corresponding author: Muchtaridi Muchtaridi (muchtaridi@unpad.ac.id)

Received 27 March 2024 ♦ **Accepted** 29 May 2024 ♦ **Published** 14 August 2024

Citation: Fakih TM, Hikmawati D, Sutedja E, Dwiyana RF, Atik N, Muchtaridi M (2024) In silico investigation of potential interleukin-8 (IL-8) and Cathelicidin (LL-37) inhibitors for rosacea treatment. Pharmacia 71: 1–12. https://doi.org/10.3897/pharmacia.71.e124099

Abstract

Emerging clinical observations underscore the correlation between interleukin-8 (IL-8) and rosacea. Increased IL-8 expression has been detected in rosacea samples, particularly in moderate to severe manifestations. This phenomenon has prompted the exploration of IL-8 as a prospective therapeutic target for rosacea treatment. To this end, a selection of compounds sourced from the ZINC database, encompassing six small molecules, was made with the intent of identifying promising lead candidates that exhibit drug-like characteristics against IL-8. Through an integrated in silico approach involving structure-guided drug design, encompassing molecular docking, molecular dynamics (MD) simulation, molecular mechanics Poisson-Boltzmann surface area (MM-PBSA) analysis, protein-peptide docking, and scrutiny of toxicity profiles, it was ascertained that the small molecule ZINC000022339916 effectively inhibits IL-8 activity. These findings present a novel lead compound that warrants further validation through in vitro, in vivo, and ongoing clinical investigations to confirm its potential for therapeutic management of rosacea.

Keywords

interleukin-8, rosacea treatment, ZINC molecules, in silico study, structure drug design

Introduction

Rosacea is a chronic skin condition characterized by facial inflammation, particularly affecting the cheeks, nose, forehead, and chin (Hilbring et al. 2022). Common symptoms include redness (erythema), swelling, visible blood vessels (telangiectasia), and the formation of pimples or bumps (pustules) (Two et al. 2015). While the exact cause

of rosacea remains unclear, several factors, including genetic, environmental, and inflammatory responses, have been implicated in its development (Zhu et al. 2023).

Interleukin-8 (IL-8) is a pro-inflammatory cytokine believed to play a pivotal role in the pathogenesis of rosacea. It is produced by various cells in the body, including skin cells, in response to inflammation and infection (Kan et al. 2020; Lee et al. 2020). The primary function of IL-8 is to attract white blood cells to infected or injured areas to aid in fighting infections and regulating the inflammatory response (Lee et al. 2021). However, in rosacea, IL-8 production can become excessive and uncontrolled, leading to chronic inflammation and the accompanying symptoms of the disease (Kim et al. 2022).

Research has indicated elevated levels of IL-8 expression in the skin of individuals with rosacea, particularly in areas exhibiting redness and swelling (Choi et al. 2023). This underscores the significant role of IL-8 in initiating and sustaining the inflammatory process in rosacea (Kim et al. 2013). Additionally, IL-8 can interact with other factors contributing to the pathogenesis of rosacea, including kallikrein-5 (KLK5), an enzyme involved in breaking down skin proteins and thought to be involved in the development of rosacea symptoms (Lee et al. 2020; Kim et al. 2022).

Researchers and the pharmaceutical industry have taken a keen interest in the significant role of IL-8 in rosacea, leading to the exploration of therapies targeting this cytokine. Previous studies have highlighted the potential usefulness of specific compounds, namely ZINC000409414675, ZINC000888088617, ZINC000888090135, ZINC000001893410, ZINC000022339916, and ZINC000012444335, in the therapeutic management of rosacea. The computational research indicates that the total binding energies obtained through MM-PBSA calculations for the ZINC compounds are as follows: –80.206 kJ/mol for ZINC000409414675, –62.856 kJ/mol for ZINC000888088617, –42.551 kJ/mol for ZINC000001893410, –82.671 kJ/mol for ZINC000888090135, –95.986 kJ/mol for ZINC000022339916, and –85.753 kJ/mol for ZINC000012444335. These values demonstrate superior performance compared to both the native ligand (–68.023 kJ/mol) and the market reference drug, azelaic acid (–41.361 kJ/mol) (Hikmawati et al. 2022).

ZINC stands out as a commercially available repository of small molecules sourced from extensive on-demand libraries numbering in the billions. Its updated database and tools facilitate exploring this expansive realm through a user-friendly interface, CartBlanche, leveraging similarity techniques that adjust efficiently with increasing molecule counts (Irwin et al. 2012). Furthermore, the revamped library incorporates data structuring techniques for swift exploration of molecules and their pertinent attributes, such as structures, partial atomic charges, c Log P values, and solvation energies (Tingle et al. 2023). As such, further investigation into the relationship between ZINC, IL-8, and rosacea is crucial to developing more effective and targeted treatments for this condition, which affects a considerable number of individuals worldwide.

In addition to IL-8, cathelicidin (LL-37) is another molecule implicated in rosacea. LL-37 is an antimicrobial peptide produced by skin cells to combat bacterial infections. However, in rosacea, LL-37 production may increase, contributing to skin inflammation and the disease's symptoms (Zhang et al. 2011). The interplay between IL-8 and LL-37 in the pathogenesis of rosacea is under study to better comprehend their roles in driving excessive skin inflammation and to aid in the development of improved treatment strategies for this condition (Kim et al. 2018).

Materials and methods

Preparation of small compounds and target molecules

The crystal structure of interleukin-8 (IL-8) was obtained from the protein data bank (PDB ID: 5D14) and subjected to energy minimization (Powers et al. 1993). The crystal structure of the protein was examined for missing atoms, alternative locations, the addition of water molecules, the presence of multiple molecules, chain breaks, and other anomalies. Polar hydrogen atoms were added, and Kollman united atom charges were assigned. The chemical structures of the small molecules (ZINC000409414675, ZINC000888088617, ZINC000888090135, ZINC000001893410, ZINC000022339916, and ZINC000012444335) used in the study were retrieved from the ZINC database (https://zinc.docking.org/) (Hikmawati et al. 2022). The preparation process involved the use of ChemDraw Professional 16.0 and Chem3D 16.0 software (Lumbanraja et al. 2023). The three-dimensional molecular structures were designed and refined using the Quantum ESPRESSO v.7.1 program with density functional theory (DFT) methodology. Becke's potential function theory (B3LYP) with 3 parameters and the 3–21G basis set were employed for calculations (Giannozzi et al. 2020).

Prediction of the biological activity of small compounds

The chemical structure identification of the small molecules utilized in the study was conducted using chemical analysis by accessing the prediction of activity spectra for substances (PASS) web server, accessible through the URL http://www.way2drug.com/passonline/ (Lagunin et al. 2000). The PASS platform employs an algorithm capable of identifying interactions between chemical compounds and the target protein under examination. This tool assesses the potential of a chemical compound to act as an inhibitor or agonist for the specified target protein. To perform PASS predictions, the molecular structure data of the compound is input using its SMILES or InChI representation. Subsequently, the platform predicts the compound's activity spectrum based on the probable activity (Pa) and probable inactivity (Pi) values, aiming to evaluate its potential activity against the target protein (Islam et al. 2022). The Pa value represents the likelihood of the chemical compound demonstrating

the desired activity on the target protein. A higher Pa value indicates a greater likelihood of the compound displaying the desired activity. This Pa value serves as an indicator of the potency of the chemical compound as an inhibitor or agonist for the tested target protein. On the other hand, the Pi value signifies the likelihood of the chemical compound exhibiting undesirable activity on the target protein. A higher Pi value suggests an increased possibility of the compound displaying undesired activity. This Pi value serves as an indicator of potential interactions between chemical compounds and unintended target proteins, as well as potential side effects that might arise.

Molecular docking and molecular dynamics simulations of small compounds against IL-8

Molecular dynamics simulations and molecular docking were conducted using the Ubuntu 23.04.5 LTS operating system on a Dell workstation equipped with an Intel Core i5–11400 CPU (12 MB cache, up to 4.40 GHz) processor and an NVIDIA GeForce GTX 1080 Ti graphics card. The system had 64 GB of RAM, a 256 GB SATA HDD, and a 256 GB SSD NVME. The docking process involved AutoDock 4.2 from MGLTools (https://ccsb.scripps.edu/mgltools/) for blind docking of all small molecules with IL-8 (Forli et al. 2012). The grid dimensions for X, Y, and Z coordinates were set at 64, 60, and 60, respectively, with a central grid placement at 2.390, 17.146, and –3.842. The grid spacing was maintained at 1.00 Å with an exhaustiveness of 8. Molecular dynamics simulations were carried out using GROMACS 2016.3 (Aragones et al. 2013). To visualize, assess, and analyze molecular dynamics trajectories, various software tools were employed, including PyMOL 3.0 (Delano 2002), QtGrace (Adnan et al. 2022), Visual Molecular Dynamics (VMD) v.1.9.4 (Humphrey et al. 1996), and Discovery Studio Visualizer v.2021 (BIOVIA 2005). The simulations of IL-8-ZINC complex molecular dynamics (200 ns) were performed using the AMBER-FF14SB-ILDN force field within GROMACS 2016.3, employing molecular mechanics at a temperature of 300 K (Gül and Pehlivan 2018). Sampling of conformations occurred at intervals of 10 ps during the 200 ns simulations for the IL-8-ZINC complex. The GROMACS 2016.3 utilities, gmx rms, gmx rmsf, gmx gyrate, gmx sasa, gmx rdf, and gmx hbond, were utilized for trajectory analysis, including root mean squared deviation (RMSD), root mean squared fluctuation (RMSF), radius of gyration (Rg), radial distribution function (RDF), surface area solvent accessible (SASA), secondary structure determination, and hydrogen bond (HBond) analysis. QtGrace was employed to create graphs and figures for visualization and presentation of the obtained data.

MM-PBSA binding energy calculation

The process of calculating interaction-free energy involved employing the Molecular Mechanics/Poisson Boltzmann Surface Area (MM-PBSA) method, which is a well-established approach for analyzing molecular interactions within biological systems (Tuccinardi 2021). The MM-PBSA calculation was facilitated using specific molecular dynamics scripts tailored for this purpose. To compute the binding free energies within the MM-PBSA framework, the g_mmpbsa script provided by the GROMACS 2016.3 software package was utilized. This approach allows for a comprehensive assessment of the energetics of interactions between biomolecules and contributes to a deeper understanding of their behavior and stability.

Protein-peptide molecular docking study against LL-37

Molecular docking was executed using IL-8, extracted from the final trajectory of a 200 ns molecular dynamics simulation, in conjunction with cathelicidin (LL-37). The crystal structure of LL-37 was sourced from the Protein Data Bank (PDB ID: 2K6O) and prepared accordingly (Wang 2008). The assessment of protein-peptide interactions involved employing the PatchDock server (http://bioinfo3d.cs.tau.ac.il/PatchDock/) (Schneidman-Duhovny et al. 2005). The grouping procedure adhered to the default root mean square deviation (RMSD) with a maximum threshold of 2.00 Å. The chosen complex type was the protein-peptide configuration. PatchDock utilizes well-suited algorithms to generate surface representations of molecules, presenting them in convex, concave, and planar forms. Subsequent optimization is applied to small-sized molecules within PatchDock, resulting in a collection of stable complexes. During this process, adjustments are made to the relative orientation of molecules, limiting the flexibility of surface side chains involved in interactions while allowing controlled motion for small, rigid entities. The top 10 candidate solutions underwent a re-evaluation based on the PatchDock score and atomic contact energy (ACE) score (Li et al. 2022). The identification of molecular protein-peptide docking outcomes hinged on the scores attained through this approach. The visual representation of interactions and binding within the docked conformation was facilitated using the Discovery Studio Visualizer v.2021 software tool.

Prediction of small compound toxicity profiles

Toxicity prediction is a procedure employed to assess the potential toxic effects of the molecular composition of small compounds before embarking on clinical trials involving humans or animals. Among the methodologies employed for toxicity prediction, one notable approach is the preADMET 2.0 (prediction of ADME and TOXicity) server (https://preadmet.webservice.bmdrc.org/) (Eurtivong et al. 2019). PreADMET 2.0 serves to assess the potential toxicity of bioactive compounds by scrutinizing their pharmacokinetic characteristics. These characteristics encompass the absorption, distribution, metabolism, excretion, and interaction of small-molecule compounds with receptor proteins. The preADMET 2.0 method employs statistical techniques and machine learning algorithms to analyze the pharmacokinetic traits of molecular compounds.

Results

IL-8 macromolecule crystal structure and energy minimization process

The crystal structure of Interleukin-8 (IL-8), obtained from the Protein Data Bank (PDB ID: 5D14), was subjected to energy minimization to optimize its conformational stability. This process was carried out using the GROMACS 2016.3 software, applying the AMBER-FF14SB-ILDN force field parameters. The goal was to mitigate any excess energy present in loops, sheets, and bonds within the protein structure. Subsequently, the optimized structure was superimposed using Discovery Studio Visualizer v.2021 to visualize any deviations in comparison to the initial structure. The root mean squared deviation (RMSD) was calculated to quantify the structural changes, resulting in a calculated RMSD value of 1.260 Å. This value indicates that the structure underwent minimal conformational alterations during the energy minimization process (Fig. 1). This assessment highlights the stability of the structure after energy minimization.

Small compounds chemical structure and biological activity properties

Biological activity prediction entails assessing the potential biological effects of bioactive compounds prior to initiating clinical trials in humans or animals. This process aims to identify compounds that might exhibit desired biological activities before embarking on more intricate and costly experimental evaluations. The biological activity of each bioactive compound is forecasted using the Prediction of Activity Spectra for Substances (PASS) web server. Based on the outcomes of the biological activity prediction in Table 1, it is evident that only a select few small-molecule compounds exhibit biological activity against IL-8, including ZINC000022339916 and ZINC000012444335. As such, the ZINC compounds are postulated to possess activity against IL-8. IL-8 is a proinflammatory cytokine with a role in stimulating immune responses and inducing inflammation within the body. The forecasted biological activity serves as an invaluable initial step in guiding the selection and development of potential candidate compounds for medicinal and therapeutic applications.

Table 1. Assessment of the prospective predictive capacity of the biological activity associated with the small-molecule structures.

Small molecules	Potential activity (Pa)	Potential inactivity (Pi)	Possible activity
Azelaic Acid	0.610	0.005	Interleukin 2 agonist
	0.339	0.011	Interleukin agonist
	0.303	0.014	Interleukin 10 agonist
	0.253	0.037	Interleukin 6 antagonist
	0.182	0.003	Interleukin 1a antagonist
	0.144	0.014	Interleukin 12 agonist
	0.133	0.070	Interleukin 4 antagonist
	0.065	0.006	Interleukin 1 beta converting enzyme inhibitor
ZINC000409414675	–	–	–
ZINC000888088617	–	–	–
ZINC000001893410	–	–	–
ZINC000888090135	–	–	–
ZINC000022339916	0.482	0.004	Interleukin agonist
	0.351	0.003	Interleukin 12 agonist
	0.111	0.065	Interleukin 2 antagonist
ZINC000012444335	0.284	0.040	Interleukin antagonist
	0.152	0.061	Interleukin 1 antagonist
	0.127	0.036	Interleukin 2 antagonist
	0.104	0.038	Interleukin 5 antagonist

All the investigated small-molecule compounds in this study also exhibited a likelihood of activity against various interleukins, with their biological activity indicated by the dominant Pa values over the Pi values. Moreover, the Pa values of the compound molecules fall within the range of 0.104 to 0.482. The notion of potential activity is employed to assess the inherent capability of small compound molecules to induce desired biological effects. Conversely, the Pi values of the compound molecules range from 0.003 to 0.065. The concept of inactivity potential pertains to instances where a small compound molecule fails to display activity or does not function effectively.

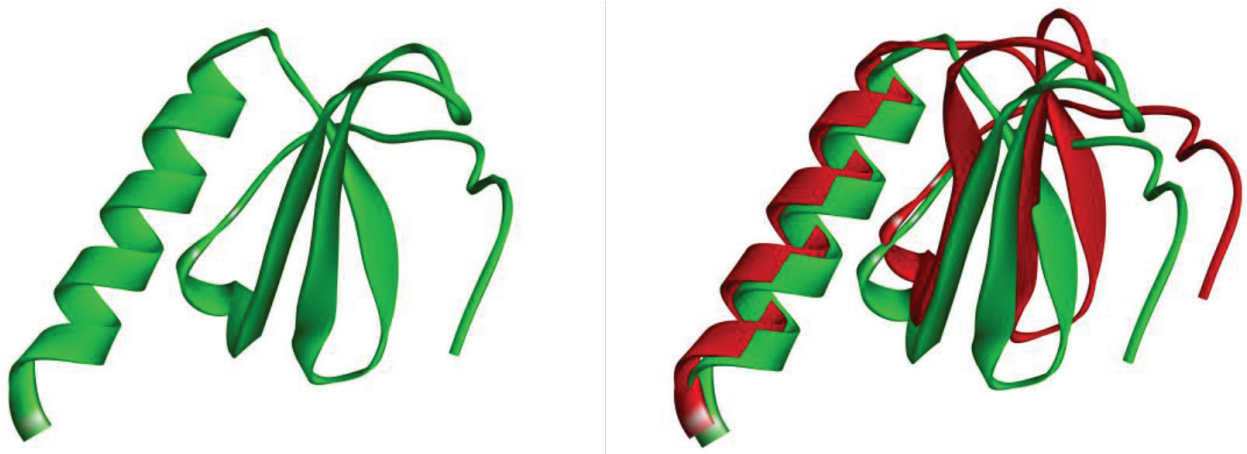

Figure 1. The cartoon depiction of IL-8 (PDB ID: 5D14) is presented on the left side, represented in green. On the right side, the superimposed IL-8 structure is displayed, with the original structure shown in green and the energy-minimized structure in red.

Investigation of the interactions between IL-8 and small compounds

The molecular docking analysis was employed to assess the binding affinity, binding energy, and potential intermolecular interactions between IL-8 and the remaining amino acids. This analysis aimed to evaluate the distances and bond conformations of these interactions. By combining all the listed small molecules with IL-8, we examined their binding affinity. The comprehensive details of the ZINC compound molecules, including binding energy and inhibition constant, are presented in Table 2. Notably, a high binding affinity was observed for certain small molecules, such as ZINC000001893410 (–7.35 kcal/mol) and ZINC000022339916 (–7.58 kcal/mol), which also displayed significant interactions with conventional amino acids. The investigation revealed that these two ZINC compound molecules acted as robust inhibitors of IL-8, as outlined in Table 2. The molecular structures of ZINC000001893410 and ZINC000022339916 are illustrated in Fig. 2.

Table 2. Small compounds that exhibit an attraction to IL-8 and possess specific binding characteristics.

Small molecules	Target macro-molecule	Binding affinity	Inhibition constant (Ki)
Azelaic Acid	IL-8	–7.21 kcal/mol	5.19 uM (micromolar)
ZINC000409414675		–6.15 kcal/mol	31.10 uM (micromolar)
ZINC000888088617		–5.51 kcal/mol	90.80 uM (micromolar)
ZINC000001893410		–7.35 kcal/mol	4.12 uM (micromolar)
ZINC000888090135		–5.55 kcal/mol	85.72 uM (micromolar)
ZINC000022339916		–7.58 kcal/mol	2.78 uM (micromolar)
ZINC000012444335		–7.19 kcal/mol	5.36 uM (micromolar)

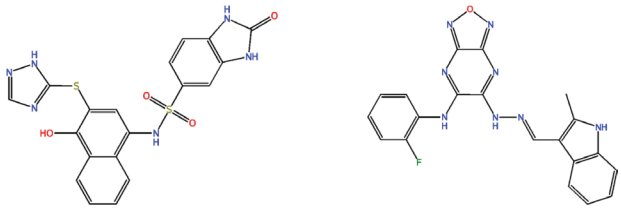

Figure 2. Structures of small molecules: ZINC000001893410 (on the left) and ZINC000022339916 (on the right).

In Fig. 3, a visual representation illustrates how the chemical structural complexes of several different small compounds (ZINC000409414675, ZINC000888088617, ZINC000888090135, ZINC000001893410, ZINC000022339916, and ZINC000012444335) form. These complexes hinder the binding accessibility of small-molecule compounds through interactions that inhibit binding in that specific area. Subsequently, we conducted a molecular docking analysis involving IL-8 and these small compounds. The primary goal was to identify the most favorable docking position across the entire surface of the protein target (Fig. 3). The results of this analysis uncovered a notable binding pattern between the ZINC group's small molecules and the central region of the IL-8 molecule. This finding strongly suggests a high potential for interaction between the two entities.

Moreover, an examination was conducted on the bonding arrangement between IL-8 and molecules of the ZINC compound, specifically focusing on ZINC000001893410 and ZINC000022339916. The findings indicate the presence of numerous potent amino acid residues within IL-8, capable of establishing hydrogen linkages with ZINC000001893410 and ZINC000022339916 at optimal bond distances (Fig. 3). Ultimately, it was deduced that ZINC000001893410 predominantly forges the majority of interactions (typical hydrogen bonds) with IL-8's amino acid residues LYS21, LEU23, VAL25, GLN57, and GLU61. These hydrogen bonds are arranged geometrically around IL-8's active site. Besides hydrogen bonds, IL-8 also generates hydrophobic associations with ZINC000001893410 through LEU23, VAL25, VAL60, and LEU64.

Nonetheless, the ZINC000022339916 small molecule predominantly establishes the majority of interactions (typical hydrogen bonds) with IL-8's amino acid residues LEU23, VAL25, and GLU61. These hydrogen bonds trigger the creation of stable molecular linkages encircling IL-8's active site. Beyond hydrogen bonds, IL-8 also generates hydrophobic partnerships with ZINC000022339916 via LEU23, ARG24, VAL25, and VAL 60. The involvement of hydrogen bonds and hydrophobic interactions contributes to fortifying the IL-8-ZINC complex and offers insights into ZINC000022339916's potential as an effective inhibitory agent. As such, the synergic merging of these two interaction types could yield significant ramifications in advancing therapeutics or therapeutic strategies centered on the IL-8-ZINC complex, particularly in intervening within biological processes associated with IL-8.

Interaction between IL-8 and ZINC small-molecule complexes in motion

Molecular dynamics simulations spanning 200 ns were employed to comprehend alterations in conformation, stability, and interactions within the free IL8-ZINC complex. Prior to commencing the molecular dynamics analysis, the IL8-ZINC complex's average potential energy in its free state was determined. Table 3 enlists the values for RMSD, RMSF, SASA, Rg, and RDF. The process of ligand binding to target molecules can introduce modifications to structure and stability and even induce conformational shifts. RMSD values serve as indicators of structural deviations and stability (Ramadhan et al. 2022). For the IL-8-ZINC complex, the observed RMSD values fluctuated between 0.285327 nm and 0.430443 nm (Table 3). The RMSD plot unveiled the attachment of the ZINC small molecule within IL-8's binding pocket, which led to limited deviations in structure and conformation when

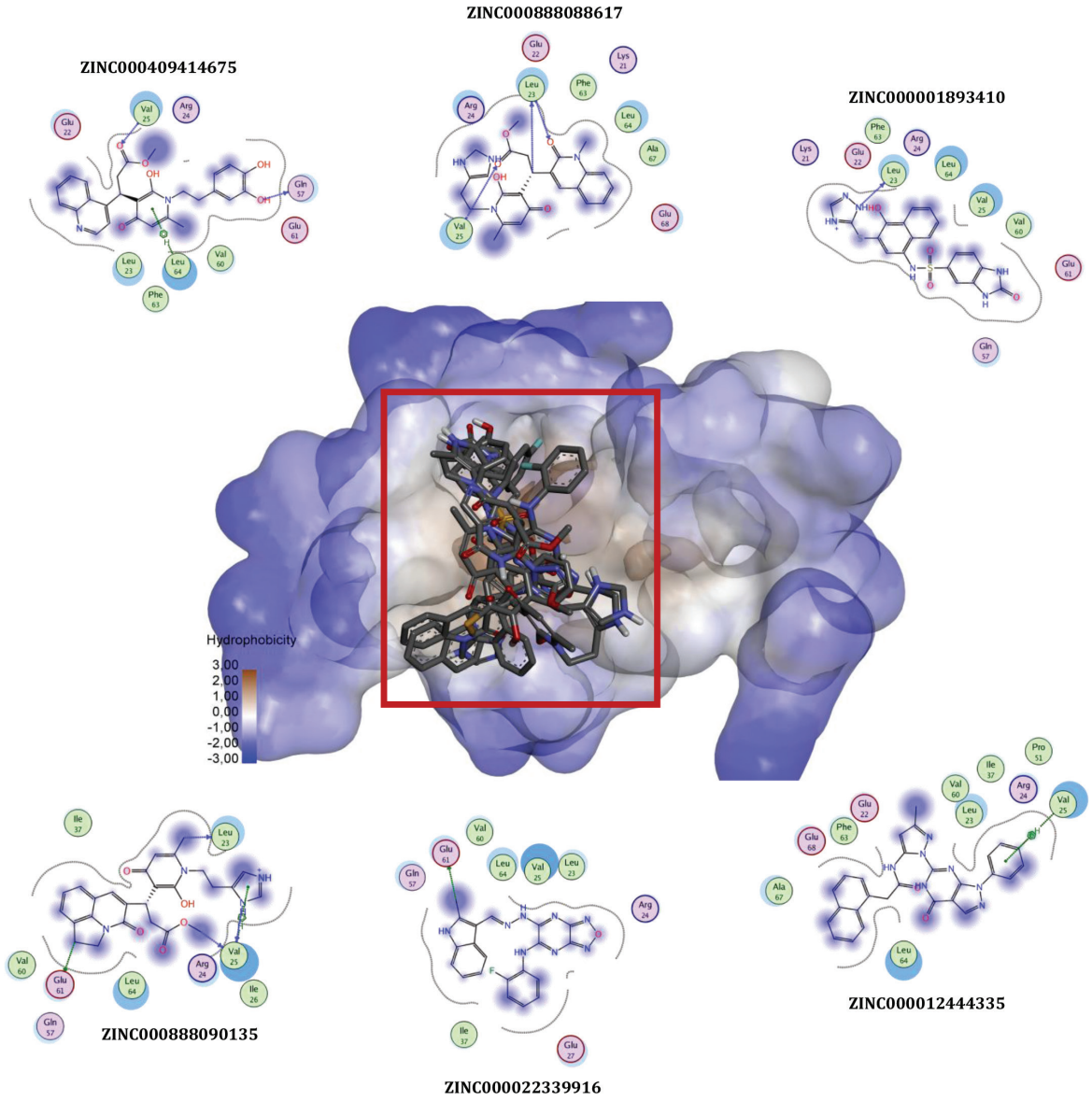

Figure 3. Illustration of the IL-8-ZINC compound complex portrayed using a surface depiction. ZINC's compact molecules are visualized as colored projections. A closer examination of the IL-8 binding region is displayed, highlighting pivotal amino acid constituents responsible for establishing connections with the inhibitory ZINC molecule.

Table 3. The MD parameters for the IL-8-ZINC system were computed upon the conclusion of the simulation.

Small molecules	Average RMSD (nm)	Average RMSF (nm)	Average Rg (nm)	Average SASA (nm^2)	Average RDF (g(r))
Azelaic Acid	0.314993	0.181963	1.26563	56.32126	4.44697
ZINC000409414675	0.346895	0.174753	1.25559	57.66862	4.38007
ZINC000888088617	0.315445	0.198111	1.27439	57.04734	3.57715
ZINC000001893410	0.285327	0.150351	1.26010	56.23075	4.31822
ZINC000888090135	0.312345	0.147937	1.25898	55.84815	3.97108
ZINC000022339916	0.430443	0.204091	1.28771	56.50664	4.41068
ZINC000012444335	0.293000	0.153917	1.27114	55.97373	3.91619

compared to the original IL-8 configuration (Fig. 4). However, minor fluctuations were noticeable due to the initial alignment of ZINC with the IL-8 binding pocket. Following these initial shifts, a state of equilibrium emerged, and the system remained stable throughout the simulation. Simulation outcomes conclusively demonstrated that the presence of ZINC compound molecules binding to IL-8 did not induce changes in the stability or structure of IL-8. The RMSD values were consistently low during several segments of the simulation, maintaining equilibrium and indicating the stability of the IL-8-ZINC complex (Fig. 4).

The variability in the local structure of the IL-8-ZINC complex was assessed through the employment of RMSF values, graphically presented in Fig. 4. A compilation of RMSF values can be found in Table 3, encapsulating the average fluctuation of residues. This comprehensive representation elucidates notable fluctuations within diverse regions of the IL-8 structure. While the simulations exhibited scarce binding of the ZINC small molecule, the binding of ZINC000022339916 to IL-8 induced sporadic, unpredictable residual fluctuations (Fig. 4). In the pursuit of a deeper comprehension of a protein's tertiary

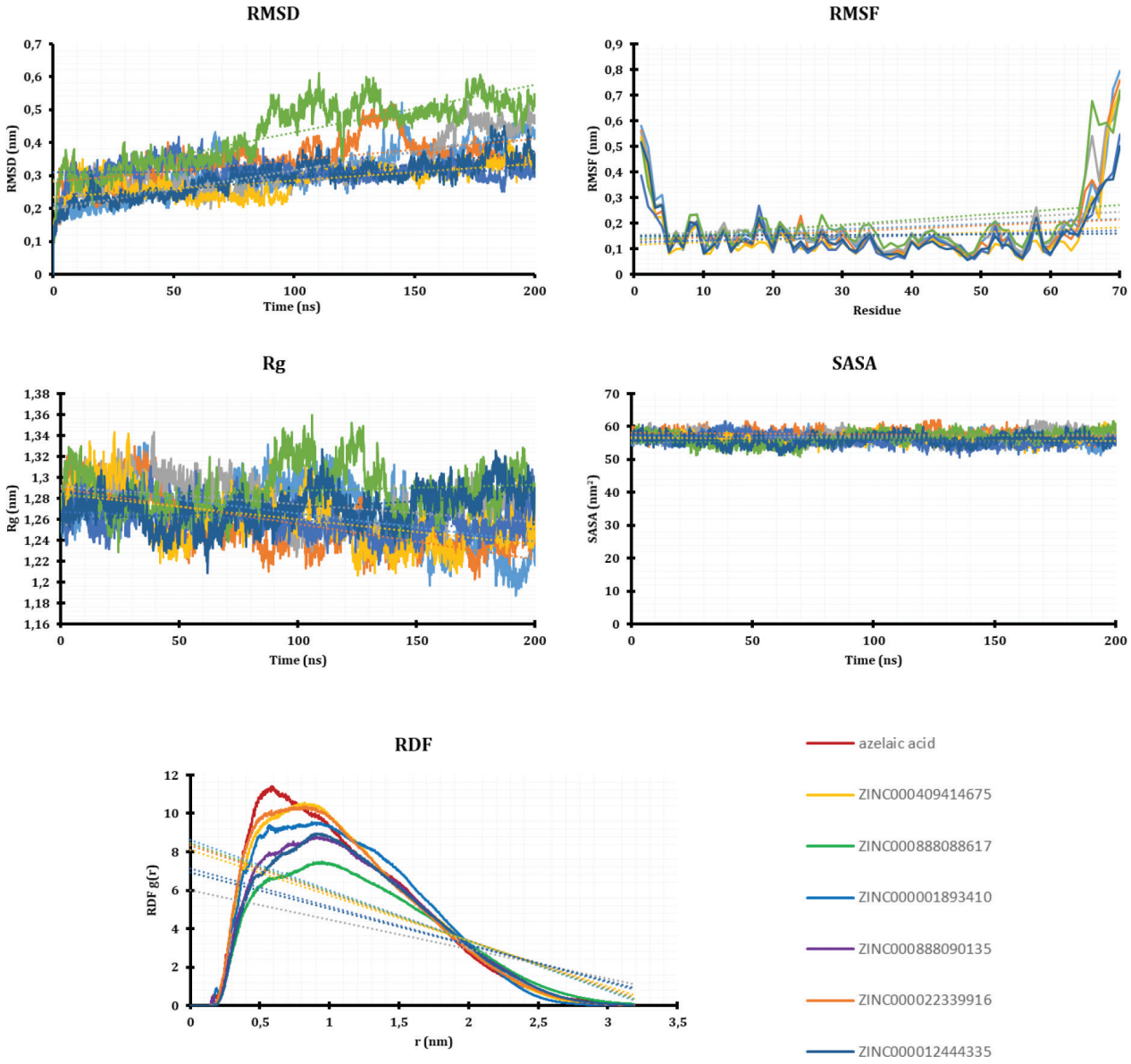

Figure 4. Dynamic changes in the structure of IL-8 upon ZINC binding. Plot illustrating the RMSD of the IL-8-ZINC complex over time. Representation of the RMSF of IL-8 post-binding. Evolution of the Rg for the IL-8-ZINC complex over time. Presentation of the SASA of the IL-8-ZINC complex across time. A visual depiction of the RDF for IL-8 after binding. These values have been derived from a 200 ns MD simulation timeframe. Each color signifies the value obtained for the free IL8-ZINC complex.

structure volume and overall conformational profile, the calculation of Rg is pursued, serving as a gauge of protein stability within a biological context. A heightened Rg value signifies increased flexibility in protein arrangement (Muchtaridi et al. 2023). The calculated average Rg values for the IL8-ZINC complex were observed to range from 1.25559 nm to 1.28771 nm, respectively (Table 3). Subtle deviations in the Rg plot were noticeable within the IL8 structure upon interaction with the ZINC compound molecule, signifying cohesion within the complex ensemble. Initial Rg plots displayed considerable compactness, potentially attributed to the tightly packed IL-8 configuration, while subsequent simulations demonstrated a balanced Rg equilibrium for IL8 (Fig. 4). Importantly, in the Rg plot, the incorporation of the ZINC small molecule displayed minimal structural variance and no discernible conformational transformation within IL-8. Notably, throughout the simulations, IL-8 maintained structural integrity even after the binding of the ZINC compound on a molecular level.

Subsequently, the assessment of the protein's interaction surface area with the surrounding solvent was conducted via 200 ns molecular dynamics simulations, focusing on SASA. SASA and a protein's Rg exhibit a direct correlation. Subsequent observation of the mean SASA values yielded a range between 55.84815 nm² and 57.66862 nm² for the IL-8-ZINC complex, as depicted in Fig. 4. The higher SASA value within the IL-8-ZINC complex might stem from conformational changes that expose a marginal portion of IL-8 residues to the solvent environment. Moreover, the RDF was employed to quantify atom distribution within the simulated protein

structure. Illustrated in Fig. 4, the RDF profile displayed minimal differentiation from the Rg chart. The RDF outcome suggests that the small molecule ZINC outperforms azelaic acid throughout the 200 ns MD simulation. RDF fluctuations could potentially signify alterations in protein conformation arising from interactions with ligands, environmental variations, or thermal processes. Furthermore, RDF can discern the nature of interactions occurring within proteins; a decrease in RDF implies hydrophobic interactions, while an increase indicates hydrophilic interactions (Hidayat and Fakih 2021).

Moreover, the kinetic energy of the solvent system, density, and volume, along with enthalpy and potential energy, are discerned and documented in Table 4. Over the course of the 200 ns MD simulation period, a notable dominance in kinetic energy, enthalpy, and potential energy was observed in relation to the compound molecule ZINC000012444335. This occurrence underscores the significant role these compounds play in steering system dynamics. This analytical endeavor was pursued with the intent of unveiling the pivotal contribution offered by the ZINC000012444335 compound to the interactions and transformative processes witnessed throughout the MD simulation experiment.

Evaluation of MM-PBSA and the occupancy of hydrogen bonds (HBond) calculations

Table 5 displays the mean values of liberated binding energies along with their corresponding standard deviations. The outcomes of the MM-PBSA analysis suggested that all types of energy facilitate the interaction between IL-8 and the diminutive ZINC molecule. On the whole, the IL-8-ZINC complex displayed a more robust attraction compared to the IL-8 complex coupled with azelaic acid. Notably, the diminutive ZINC000022339916 molecule manifests a liberated binding energy of –165.451 kJ/mol. This discovery portrays that the compound's molecular arrangement significantly contributes to the heightened bonding and more potent interactions between IL-8 and ZINC, positioning it as a promising contender for a potential inhibitory agent within the pertinent context.

The primary energies governing the interaction between IL-8 and ZINC compound molecules are van der Waals forces, electrostatic interactions, and the accessibility of solvent-exposed surfaces (surface area of solvent accessibility, or SASA). This phenomenon can be attributed to the attractive van der Waals forces operating between neighboring atoms within the IL-8-ZINC complex, as well as the electrostatic interactions that arise between charged groups present in both entities. Furthermore, the extent of surface area accessible to solvent molecules (SASA) assumes a vital role in facilitating contacts and interactions between these molecular constituents (Settanni et al. 2017). The amalgamation of these factors engenders an environment conducive to robust and enduring interactions between IL-8 and ZINC compound molecules within the intricate complex.

While the IL-8-ZINC interaction unfolded, an investigation into hydrogen bond formations within the complex was concurrently conducted. Across all complex systems, hydrogen bonds were identified with an occupancy rate exceeding 10%. Notably, ZINC000888090135 (at 75.48%) and ZINC000001893410 (at 88.17%) exhibited elevated hydrogen bond occupancy rates (Table 6). Remarkably, both demonstrated a distinctive characteristic of engaging in hydrogen bond formations with the same residues as those interacting with azelaic acid, specifically GLN6, LYS9, SER12, LYS13, ARG45, GLU46, and CYS48 located at the IL-8 binding site. This signifies a parallel interaction pattern concerning the development of hydrogen bonds between specific ZINC molecules and IL-8 within their binding pocket.

Table 4. The MD output profile for the IL-8-ZINC complex was computed upon completion of the simulation.

Small molecules	Kinetic energy (kJ/mol)	Potential energy (kJ/mol)	Enthalpy (kJ/mol)	Volume (nm^3)	Density (kg/m^3)
Azelaic Acid	–11.3051	–13.1707	–24.4761	268.403	996.894
ZINC000409414675	–1.22068	–57.6425	–58.8698	268.129	997.788
ZINC000888088617	14.3595	4.75488	19.1112	268.732	997.492
ZINC000001893410	0.955852	–35.3305	–34.3806	268.106	997.873
ZINC000888090135	10.6246	1.75869	12.3863	268.013	997.787
ZINC000022339916	4.66478	–19.347	–14.6841	268.259	997.55
ZINC000012444335	–5.35918	–112.975	–118.34	268.201	997.751

Table 5. Determination of the binding free energy within the IL8-ZINC complex using MM-PBSA calculations.

Complex	Ebinding (kJ/mol)	SASA (kJ/mol)	Epolar Solvation (kJ/mol)	EElectrostatic (kJ/mol)	EVan der Waals (kJ/mol)
IL-8-Azelaic Acid	–42.564	–9.621	78.858	–36.376	–75.425
IL-8-ZINC000409414675	–91.817	–16.884	107.572	–30.961	–151.544
IL-8-ZINC000888088617	–58.453	–12.401	94.276	–29.405	–110.923
IL-8-ZINC000001893410	–50.813	–13.700	135.870	–55.334	–117.649
IL-8-ZINC000888090135	–50.216	–13.649	132.359	–59.054	–109.872
IL-8-ZINC000022339916	–165.451	–14.252	104.826	–129.620	–126.405
IL-8-ZINC000012444335	–63.311	–13.221	74.339	–4.688	–119.742

Table 6. Analysis of the intermolecular hydrogen bonding interaction between ZINC and IL-8.

Complex	Hydrogen bond (HBond) occupancy	Residue
IL-8-Azelaic Acid	60.05%	GLN6, LYS9, SER12 LYS13, ARG45, GLU46, CYS48
IL-8-ZINC000409414675	25.18%	VAL25, GLU27, ASN34, THR35, PRO51, LYS52, GLN57, GLU61, GLU68, ASN69
IL-8-ZINC000888088617	16.10%	LYS1, GLU22, LEU23 VAL25, GLU27, HIS31, ARG66, ALA67, GLU68, ASN69
IL-8-ZINC000001893410	88.17%	GLU22, LEU23, VAL25, GLU27, GLN57, GLU61, ALA67, GLU68, ASN69
IL-8-ZINC000888090135	75.48%	LEU23, VAL25, GLU27, LYS65
IL-8-ZINC000022339916	6.80%	LEU23, VAL25, ASP50, PRO51, LYS52, GLN57, GLU61, PHE63, LEU64, LYS65, ARG66, GLU68, ASN69
IL-8-ZINC000012444335	6.00%	LEU23, GLU27, THR35, GLN57, GLU61

Recognition of the molecular interactions between IL-8 and ZINC in contrast to LL-37

Protein-peptide docking was conducted to explore the binding of LL-37 to each IL-8-ZINC complex. The atomic contact energy (ACE) score was employed to evaluate the binding strength of LL-37. To enhance the credibility of the docking technique, a validation step was executed using PatchDock. This validation strategy encompassed a re-docking approach, wherein LL-37 was reconstructed to match its original crystal structure. Throughout this re-docking process, close attention was paid to RMSD values and active sites. Additionally, potential binding residues of LL-37 were identified. The outcomes of the method validation phase furnish valuable insights into the precision and efficacy of protein-peptide docking simulations, thereby establishing the dependability of subsequent analyses that assess the interplay between LL-37 and the IL-8-ZINC complex.

This investigation unveiled intriguing outcomes concerning the interplay between complexes of small molecules (ZINC000409414675, ZINC000888090135, ZINC000022339916, and ZINC000012444335) and IL-8 concerning LL-37 (Table 7). In this specific context, the favorable scores generated by the PatchDock analysis are captivating, characterized by binding energies spanning from 94.30 kJ/mol to 366.04 kJ/mol. These findings suggest that the trio of small molecules possesses the capability to effectively impede the binding of LL-37 to the surface of IL-8. Moreover, these results unlock the potential utility of these three compounds as potent inhibitors of IL-8.

Investigation of the toxicity characteristics of small compounds

To ensure the safety of the ZINC small molecule, a toxicity prediction process is conducted, as it can aid in evaluating the safety and efficacy of a drug even before its administration to humans or experimental animals. The evaluation of absorption, distribution, metabolism, and excretion (ADME) along with toxicity is conducted utilizing an online platform known as preADMET 2.0. For absorption, predictions are made for human intestinal absorption (HIA) and Caco-2 cell permeability. Distribution assessments encompass plasma protein binding (PPB) and blood-brain barrier (BBB) permeability, while toxicity profiles are examined for carcinogenic and mutagenic effects. The HIA value serves as an indicator of the extent to which the active substance is absorbed in the human intestine. Based on the percentage of HIA, a compound is classified as well absorbed (70–100%), moderately absorbed (20–70%), or poorly absorbed (0–20%) (Wadapurkar et al. 2018). As depicted in Table 8, the ZINC compound molecules, on the whole, align with the specified range criteria.

Moreover, the utilization of Caco-2 cell modeling was employed to anticipate the absorption of active compounds through the oral route in a controlled in vitro setting. The notable permeability of Caco-2 cells is reflected by values surpassing 0.9 x 10^{-6} cm/s (Mohapatra et al. 2015). Solely the compound molecule ZINC000001893410 exhibits a Caco-2 cell value beneath 0.9 x 10^{-6} cm/s, signifying limited permeability in terms of cellular membrane penetration. The plasma protein binding (PPB) value exerts an impact on the pharmacokinetic and pharmacodynamic attributes of drugs. A PPB value surpassing 90% suggests a strong binding affinity between the drug and plasma proteins, whereas a PPB value below 90% indicates a weaker binding propensity with plasma proteins, consequently facilitating proper distribution to the intended target sites. An additional parameter for distribution is the Blood-Brain Barrier (BBB) value, which signifies the concentration of a drug within the brain. This parameter holds significance in gauging a drug's capability to traverse the blood-brain barrier. BBB values are stratified into two categories: values exceeding 0.3 are interpreted as facile blood-brain barrier penetration, while values below –1 indicate limited distribution into the brain (Vique-Sánchez 2021).

Table 7. Findings from the molecular docking study involving LL-37 and the IL-8-ZINC complex.

Complex	PatchDock Score	ACE Score (kJ/mol)
IL-8-Azelaic Acid	9912	7.48
IL-8-ZINC000409414675	9850	94.30
IL-8-ZINC000888088617	10664	–165.79
IL-8-ZINC000001893410	10628	–392.76
IL-8-ZINC000888090135	10132	232.84
IL-8-ZINC000022339916	10036	366.04
IL-8-ZINC000012444335	10484	175.67

Discussion

In spite of progress made in molecular and computational techniques, there remains a limited exploration of diagnosing and devising treatment plans for rosacea. Adopting treatment approaches that stem from the molecular signature of the ailment represents the initial stride toward precision-oriented therapy and enhanced clinical outcomes. Utilizing molecular insights to guide rosacea treatment could potentially

Table 8. ADME characteristics at the molecular level of ZINC compounds.

Small molecules	Absorption		Distribution		Toxicity	
	HIA (%)	Caco2 (10^{-6} cm/s)	PPB (%)	BBB	Mutagenic	Carcinogenic
Azelaic Acid	72.313515	6.41343	100.000000	0.604758	+	–
ZINC000409414675	93.312647	20.1863	90.845754	0.168964	+	–
ZINC000888088617	90.951722	14.3092	91.819375	0.063003	+	–
ZINC000001893410	83.400578	0.396941	98.011034	0.061796	–	–
ZINC000888090135	91.281942	12.3984	91.800649	0.068811	+	–
ZINC000022339916	89.919244	13.4602	86.701280	0.413125	+	–
ZINC000012444335	96.355718	21.7605	92.369709	0.039689	+	–

unveil novel avenues for pinpointing more accurate therapeutic focal points, achieving a deeper grasp of the disease's fundamental mechanisms, and crafting treatment strategies that are both more potent and individualized (Ayaz et al. 2020; Khanal et al. 2021). This investigation delves into the utilization of computational algorithms in drug discovery as a potent tactic within medical research, as it expedites the identification and characterization of drug compounds. The realm of computational drug discovery encompasses all stages of drug research, spanning from targeted drug discovery and development, the pinpointing of drug targets, validation of drug-target interactions, lead discovery and process optimization, to preclinical assessments (Zhou et al. 2019). Given the expansive availability of small molecules and biological macromolecules, employing experimental biological studies to identify suitable drugs for target molecules can be a laborious and time-intensive endeavor. Currently, structure-assisted screening techniques stand as the most widely applied methodologies for unearthing small molecules that exhibit drug-like attributes.

In this research endeavor, we conducted a molecular docking investigation with the aim of pinpointing potential drug candidates that target IL-8. Our scrutiny encompassed an assessment of the binding affinity, binding energy, and conformation of bonds governing the potential interaction between the IL-8 small molecule and the residual amino acids at varying intermolecular distances. Through the outcomes of our investigation, IL-8 emerged as being modulated by ZINC000022339916, as evidenced by its notably elevated binding energy value of –7.58 kcal/mol, accompanied by noteworthy interactions with residual amino acids.

The most favorable docking orientation of small molecules on the surface of the protein involves ZINC, demonstrating a tight binding configuration within IL-8. ZINC000022339916 engages with the primary IL-8 groove through hydrogen bonding interactions (LEU23, VAL25, and GLU61) as well as hydrophobic interactions (LEU23, ARG24, VAL25, and VAL60) with specific amino acid residues. Prior literature has underscored the pivotal role of hydrogen bonding in dictating the precise binding of a ligand. The interplay between the inhibitor molecule and IL-8, fostered by hydrogen bonds and hydrophobic interactions, collectively enhances the stability of the complex. To probe into the conformational variations, interactions, and stability of the IL8-ZINC complex, extensive molecular dynamics (MD) simulations lasting 200 ns were performed. Presently, MD simulations have evolved as a valuable tool for discerning the intricate relationship between structure and function in macromolecules. The characterization of MD parameters, including RMSD, RMSF, Rg, SASA, and RDF, collectively attests to the potency of ZINC as an IL-8 inhibitor.

The impact of ligand binding on the target protein can induce structural perturbations, conformational adjustments, and fluctuations in the macromolecule's stability. The calculation of the RMSD value offers insights into the extent of structural divergence and overall stability. Comparative RMSD values suggest minimal deviation from the initial IL-8 structure upon ZINC binding, signifying the robustness of the IL-8-ZINC complex's stability. RMSF reflects the flexibility of the local structure. Initially, significant residual fluctuations within various regions of IL-8 were observed, which were subsequently mitigated during the simulation process through ZINC binding. This phenomenon reflects the structural adaptability of the IL-8-ZINC complex. Tertiary structure, volume, and the global conformation of a protein correspond with Rg. The Rg analysis highlights minimal structural divergence and a lack of conformational shifts within IL-8 upon ZINC binding. Similarly, the Rg plot indicates that IL-8 maintains a compact configuration throughout the simulation. SASA describes the outer surface area of a protein exposed to solvent interactions. Notably, the diminished SASA of the IL-8-ZINC complex does not markedly differ from that of IL-8-azelaic acid. This observation led us to hypothesize that ZINC's binding to IL-8 initiates a conformational alteration, thereby exposing internal IL-8 residues to solvent interactions.

Additionally, the evaluation of the binding energy within the IL-8-ZINC complex was undertaken via MM-PBSA analysis. The energy liberated during the interaction process or the formation of bonds between the ligand and the target molecule is presented as the binding energy. This measure stands in an inversely proportional relationship with the ligand-protein binding strength (Chéron and Shakhnovich 2017; Maier et al. 2022). The cumulative energies of electrostatics, polar solvation, solvent-accessible surface area (SASA), and van der Waals interactions constitute the ultimate binding energy (Damayanti et al. 2022; Mishra et al. 2022). The MM-PBSA analysis indicated that all these energy components contribute to the interaction between IL-8 and ZINC. Intriguingly, peptide-based molecular docking outcomes uncovered that the small-molecule compounds ZINC000888090135, ZINC000022339916, and ZINC000012444335 possess the capability to engage with IL-8, thereby impeding the attachment of LL-37. As a result of this inhibition, the prospect of interactions that might spur the progression of rosacea can be preempted or mitigated, presenting an avenue for curtailing the advancement of this condition.

Furthermore, ZINC000022339916, previously identified as an effective KLK5 inhibitor due to its superior stability compared to other ZINC compounds, azelaic acid, and the native ligand of the co-crystal KLK5, is also anticipated in this investigation to exhibit significant inhibitory properties, reaching –165.451 kJ/mol. Furthermore, it demonstrates the ability to hinder LL-37 attachment to IL-8's surface, boasting an ACE value of 366.04 kJ/mol. These results underscore the significance of the generated pharmacophore model for ZINC000022339916, highlighting its diverse features like multiple aromatic and hydrophobic groups, along with essential hydrogen bonding acceptors and donors, crucial for augmenting its efficacy as an IL-8 protein inhibitor (Hikmawati et al. 2022). Hence, preliminary findings from computational studies suggest that compounds derived from the ZINC database show potential for diverse biological therapies, including treatments for rosacea. However, further validation through both in vitro and in vivo investigations is essential to confirm their biological efficacy, validate computational forecasts, and deepen our understanding of their interaction mechanisms with pertinent biological targets.

Conclusion

Elevated IL-8 levels have been observed in connection with the rosacea condition. This underscores the pivotal role IL-8 plays in the pathological mechanism of this ailment. A heightened IL-8 level could indicate more pronounced inflammation, given IL-8's involvement in spurring the migration of inflammatory cells toward affected regions. Modulating IL-8 activity could hold promise for therapeutic approaches and drug development in managing rosacea. Through methodologies like structure-guided drug design, simulation analysis, and molecular docking, it was unveiled that the small molecule ZINC, particularly ZINC000022339916, holds potential as an IL-8 protein inhibitor. This research serves as an initial stride toward the identification of potential IL-8 inhibitors, a step that holds promise for future clinical validation and application in rosacea treatment.

Author contributions

Conceptualization, D.H., E.S., R.F.D., N.A., and M.M.; methodology, T.M.F.; software, T.M.F., and D.H.; validation, T.M.F.; formal analysis, T.M.F.; investigation, T.M.F., and D.H.; resources, D.H.; data curation, D.H.; writing–original-draft preparation, T.M.F.; writing–review and editing, D.H., E.S., R.F.D., N.A., and M.M.; visualization, T.M.F.; supervision, E.S., R.F.D., N.A., and M.M. All authors have read and agreed to the published version of the manuscript.

Acknowledgments

The author expresses gratitude to the Department of Dermatology and Venereology, Faculty of Medicine, Universitas Padjadjaran-Dr. Hasan Sadikin Hospital, and the Department of Biomedical Sciences, Faculty of Medicine, Universitas Padjadjaran.

References

Adnan M, Jairajpuri DS, Chaddha M, Khan MS, Yadav DK, Mohammad T, Elasbali AM, Al-Soud WA, Alharethi SH, Hassan MI (2022) Discovering tuberosin and villosol as potent and selective inhibitors of AKT1 for therapeutic targeting of oral squamous cell carcinoma. Journal of Personalized Medicine 12(7): 1083. https://doi.org/10.3390/jpm12071083

Aragones JL, Noya EG, Valeriani C, Vega C (2013) Free energy calculations for molecular solids using GROMACS. Journal of Chemical Physics 139: 034104. https://doi.org/10.1063/1.4812362

Ayaz Z, Zainab B, Khan S, Abbasi AM, Elshikh MS, Munir A, Al-Ghamdi AA, Alajmi AH, Alsubaie QD, Mustafa AEZMA (2020) In silico authentication of amygdalin as a potent anticancer compound in the bitter kernels of family Rosaceae. Saudi Journal of Biological Sciences 27(9): 2444–2451. https://doi.org/10.1016/j.sjbs.2020.06.041

BIOVIA DS (2005) Discovery Studio Visualizer v21.1.0.20298. BIOVIA, Dassault Systèmes.

Chéron N, Shakhnovich EI (2017) Effect of sampling on BACE-1 ligands binding free energy predictions via MM-PBSA calculations. Journal of Computational Chemistry 38(22): 1941–1951. https://doi.org/10.1002/jcc.24839

Choi CW, Keum H, Yang S, Kang BM, Kim D, Piao H, Kim JW, Kim BR, Youn, SW, Jon S (2023) Bilirubin nanomedicine alleviates inflammation and angiogenesis in a Rosacea mouse model. Advanced Therapeutics 6(4): 2200223. https://doi.org/10.1002/adtp.202200223

Damayanti MM, Rachmawati M, Widiyastuti E, Kharisma Y, Fakih TM, Arfan A, Ramadhan DSF (2022) Structure-based design through molecular dynamics approaches of the small-molecule bioactive compounds in cinnamon as interleukin-6 (il-6) inhibitors. Rasayan Journal of Chemistry 2022: 158–166. https://doi.org/10.31788/RJC.2022.1558192

Delano WL (2002) The PyMOL Molecular Graphics System. CCP4 Newsletter on Protein Crystallography 40.

Eurtivong C, Choowongkomon K, Ploypradith P, Ruchirawat S (2019) Molecular docking study of lamellarin analogues and identification of potential inhibitors of HIV-1 integrase strand transfer complex by virtual screening. Heliyon 5(11): E02811. https://doi.org/10.1016/j.heliyon.2019.e02811

Forli W, Halliday S, Belew R, Olson A (2012) AutoDock Version 4.2. Citeseer.

Giannozzi P, Baseggio O, Bonfà P, Brunato D, Car R, Carnimeo I, Cavazzoni C, De Gironcoli S, Delugas P, Ferrari Ruffino F, Ferretti A, Marzari N, Timrov I, Urru A, Baroni S (2020) Quantum ESPRESSO toward the exascale. Journal of Chemical Physics 152: 154105. https://doi.org/10.1063/5.0005082

Gül A, Pehlivan T (2018) Antioxidant activities of some monofloral honey types produced across Turkey. Saudi Journal of Biological Sciences 25(6): 1056–1065. https://doi.org/10.1016/j.sjbs.2018.02.011

Hidayat AF, Fakih TM (2021) Self-assembly of black cumin oil-based nanoemulsion on various surfactants: A molecular dynamics study. Makara Journal of Science 25(4): e8. https://doi.org/10.7454/mss.v25i4.1267

Hikmawati D, Fakih TM, Sutedja E, Dwiyana RF, atik N, Ramadhan DSF (2022) Pharmacophore-guided virtual screening and dynamic simulation of Kallikrein-5 inhibitor: Discovery of potential molecules for rosacea therapy. Informatics in Medicine Unlocked 28: 100844. https://doi.org/10.1016/j.imu.2022.100844

Hilbring C, Augustin M, Kirsten N, Mohr N (2022) Epidemiology of rosacea in a population-based study of 161,269 German employees. International Journal of Dermatology 61(5): 570–576. https://doi.org/10.1111/ijd.15989

Humphrey W, Dalke A, Schulten K (1996) VMD: Visual molecular dynamics. Journal of Molecular Graphics 14(1): 33–38. https://doi.org/10.1016/0263-7855(96)00018-5

Irwin JJ, Sterling T, Mysinger MM, Bolstad ES, Coleman RG (2012) ZINC: A free tool to discover chemistry for biology. Journal of Chemical Information and Modeling 52(7): 1757–1768. https://doi.org/10.1021/ci3001277

Islam S, Hosen MA, Ahmad S, ul Qamar MT, Dey S, Hasan I, Fujii Y, Ozeki Y, Kawsar SMA (2022) Synthesis, antimicrobial, anticancer activities, PASS prediction, molecular docking, molecular dynamics and pharmacokinetic studies of designed methyl α-D-glucopyranoside esters. Journal of Molecular Structure 1260: 132761. https://doi.org/10.1016/j.molstruc.2022.132761

Kan HL, Wang CC, Cheng YH, Yang CL, Chang HS, Chen IS, Lin YC (2020) Cinnamtannin B1 attenuates rosacea-like signs via inhibition

of pro-inflammatory cytokine production and down-regulation of the MAPK pathway. PeerJ 8: e10548. https://doi.org/10.7717/peerj.10548

Khanal J, Tayara H, Zou Q, Chong KT (2021) Identifying DNA N4-methylcytosine sites in the rosaceae genome with a deep learning model relying on distributed feature representation. Computational and Structural Biotechnology Journal 19: P1612–1619. https://doi.org/10.1016/j.csbj.2021.03.015

Kim GJ, Choi HG, Kim JH, Kim SH, Kim JA, Lee SH (2013) Anti-allergic inflammatory effects of cyanogenic and phenolic glycosides from the seed of Prunus persica. Natural Product Communications 8: 1–2. https://doi.org/10.1177/1934578x1300801221

Kim H Bin, Na EY, Yun SJ, Lee JB (2022) The effect of capsaicin on neuroinflammatory mediators of Rosacea. Annals of Dermatology 34(4): 261–269. https://doi.org/10.5021/ad.21.223

Kim M, Kim J, Jeong S won, Jo H, Park HJ (2018) Long-pulsed 1064-nm Nd: YAG laser ameliorates LL-37-induced rosacea-like skin lesions through promoting collagen remodeling in BALB/c mice. Lasers in Medical Science 33: 393–397. https://doi.org/10.1007/s10103-017-2410-8

Lagunin A, Stepanchikova A, Filimonov D, Poroikov V (2000) PASS: Prediction of activity spectra for biologically active substances. Bioinformatics 16(8): 747–748. https://doi.org/10.1093/bioinformatics/16.8.747

Lee HJ, Hong YJ, Kim M (2021) Angiogenesis in chronic inflammatory skin disorders. International Journal of Molecular Sciences 22(21): 12035. https://doi.org/10.3390/ijms222112035

Lee SG, Yoon MS, Kim DH, Shin JU, Lee HJ (2020) Hyaluronan oligosaccharides improve rosacea-like phenotype through anti-inflammatory and epidermal barrier-improving effects. Annals of Dermatology 32(3): 189–196. https://doi.org/10.5021/AD.2020.32.3.189

Li H, Yan Y, Zhao X, Huang SY (2022) Inclusion of desolvation energy into protein-protein docking through atomic contact potentials. Journal of Chemical Information and Modeling 62(3): 740–750. https://doi.org/10.1021/acs.jcim.1c01483

Lumbanraja MP, Anggadiredja K, Muhammad HN, Kurniati NF (2023) Alkaloids from *Pandanus amaryllifolius* Roxb Leaf as promising candidates for antidyslipidemic agents: An in silico study. Pharmacognosy Journal 15(1): 106–111. https://doi.org/10.5530/pj.2023.15.14

Maier S, Thapa B, Erickson J, Raghavachari K (2022) Comparative assessment of QM-based and MM-based models for prediction of protein-ligand binding affinity trends. Physical Chemistry Chemical Physics 24: 14525–14537. https://doi.org/10.1039/d2cp00464j

Mishra A, Mulpuru V, Mishra N (2022) Exploring the mechanism of action of podophyllotoxin derivatives through molecular docking, molecular dynamics simulation and MM/PBSA studies. Journal of Biomolecular Structure and Dynamics, 8856–8865. https://doi.org/10.1080/07391102.2022.2138549

Mohapatra S, Prasad A, Haque F, Ray S, De B, Ray SS (2015) In silico investigation of black tea components on α-amylase, α-glucosidase and lipase. Journal of Applied Pharmaceutical Science 5(12): 042–047. https://doi.org/10.7324/JAPS.2015.501207

Muchtaridi M, Triwahyuningtyas D, Muhammad Fakih T, Megantara S, Choi SB (2023) Mechanistic insight of α-mangostin encapsulation in 2-hydroxypropyl-β-cyclodextrin for solubility enhancement. Journal of Biomolecular Structure and Dynamics, 3223–3232. https://doi.org/10.1080/07391102.2023.2214237

Powers R, Garrett DS, Gronenborn AM, Clore GM, March CJ, Frieden EA (1993) The high-resolution, three-dimensional solution structure of human interleukin-4 determined by multidimensional heteronuclear magnetic resonance spectroscopy. Biochemistry 32(26): 6744–6762. https://doi.org/10.1021/bi00077a030

Ramadhan DSF, Siharis F, Abdurrahman S, Isrul M, Fakih TM (2022) In silico analysis of marine natural product from sponge (*Clathria* Sp.) for their activity as inhibitor of SARS-CoV-2 Main Protease. Journal of Biomolecular Structure and Dynamics 40: 11526–11532. https://doi.org/10.1080/07391102.2021.1959405

Schneidman-Duhovny D, Inbar Y, Nussinov R, Wolfson HJ (2005) PatchDock and SymmDock: Servers for rigid and symmetric docking. Nucleic Acids Research 33: W363–W367. https://doi.org/10.1093/nar/gki481

Settanni G, Zhou J, Suo T, Schöttler S, Landfester K, Schmid F, Mailänder V (2017) Protein corona composition of poly(ethylene glycol)-and poly (phosphoester)-coated nanoparticles correlates strongly with the amino acid composition of the protein surface. Nanoscale 9: 2138–2144. https://doi.org/10.1039/c6nr07022a

Tingle BI, Tang KG, Castanon M, Gutierrez JJ, Khurelbaatar M, Dandarchuluun C, Moroz YS, Irwin JJ (2023) ZINC-22—A Free Multi-Billion-Scale Database of Tangible Compounds for Ligand Discovery. Journal of Chemical Information and Modeling 63(4): 1166–1176. https://doi.org/10.1021/acs.jcim.2c01253

Tuccinardi T (2021) What is the current value of MM/PBSA and MM/GBSA methods in drug discovery? Expert Opinion on Drug Discovery 16: 1233–1237. https://doi.org/10.1080/17460441.2021.1942836

Two AM, Wu W, Gallo RL, Hata TR (2015) Rosacea: Part I. Introduction, categorization, histology, pathogenesis, and risk factors. Journal of the American Academy of Dermatology 72(5): P749–758. https://doi.org/10.1016/j.jaad.2014.08.028

Vique-Sánchez JL (2021) Potential inhibitors interacting in Neuropilin-1 to develop an adjuvant drug against COVID-19, by molecular docking. Bioorganic and Medicinal Chemistry 33: 116040. https://doi.org/10.1016/j.bmc.2021.116040

Wadapurkar RM, Shilpa MD, Katti AKS, Sulochana MB (2018) In silico drug design for *Staphylococcus aureus* and development of host-pathogen interaction network. Informatics in Medicine Unlocked 10: 58–70. https://doi.org/10.1016/j.imu.2017.11.002

Wang G (2008) Structures of human host defense cathelicidin LL-37 and its smallest antimicrobial peptide KR-12 in lipid micelles. Journal of Biological Chemistry 283(47): P32637–32643. https://doi.org/10.1074/jbc.M805533200

Zhang J, Xu X, Rao N V., Argyle B, McCoard L, Rusho WJ, Kennedy TP, Prestwich GD, Krueger G (2011) Novel sulfated polysaccharides disrupt cathelicidins, inhibit rage and reduce cutaneous inflammation in a mouse model of rosacea. PLoS ONE 6(2): e16658. https://doi.org/10.1371/journal.pone.0016658

Zhou L, Han FY, Lu LW, Yao GD, Zhang YY, Wang XB, Lin B, Huang XX, Song SJ (2019) Isolation of enantiomeric furolactones and furofurans from *Rubus idaeus* L. with neuroprotective activities. Phytochemistry 164: 122–129. https://doi.org/10.1016/j.phytochem.2019.05.008

Zhu W, Hamblin MR, Wen X (2023) Role of the skin microbiota and intestinal microbiome in rosacea. Frontiers in Microbiology 14. https://doi.org/10.3389/fmicb.2023.1108661